Proceedings of the ASME 2013 International Mechanical Engineering Congress & Exposition
IMECE2013
November 13-21, 2013, San Diego, California, USA

IMECE2013-66428

TOWARDS THERMAL CHARACTERIZATION OF PICO-LITER VOLUMES USING THE 3OMEGA METHOD

Shilpi Roy
Department of Electrical Engineering
Stanford University
Stanford, CA, USA
shilpir@stanford.edu

Takashi Kodama
Department of Mechanical Engineering
Stanford University
Stanford, CA, USA
kodama@stanford.edu

Srilakshmi Lingamneni
Department of Mechanical Engineering
Stanford University
Stanford, CA, USA
sril@stanford.edu

Matthew A. Panzer
KLA-Tencor Corporation
Milpitas, CA, USA
matthew.panzer@kla-tencor.com

Mehdi Asheghi
Department of Mechanical Engineering
Stanford University
Stanford, CA, USA
masheghi@stanford.edu

Kenneth E. Goodson
Department of Mechanical Engineering
Stanford University
Stanford, CA, USA
goodson@stanford.edu

ABSTRACT

The continued efforts in the biological community to optimize methodologies such as PCR and to characterize biological reactions and processes are motivating reductions in sample volume. There is a growing need for the detection of thermal phenomena in these small volumes, such as the heat released by recombination and the effective conductivities and capacities in extremely small fluidic regions. While past work has focused largely on heat transport in essentially bulk fluid volumes, there is a need to scale these techniques to the much smaller volumes of interest for biological and biomedical research."

This work applies the 3ω measurement technique to μL volumes by using heaters with dimensions of 200-700μm in lengths and 2-5μm in widths. We investigate fluid samples of DI water, silicone oil, and a salt buffer solution to experimentally determine their temperature-dependent thermal properties from 25°C to 80°C. Validation is achieved through comparison of these values of thermal conductivity κ and volumetric heat capacity C_v to literature. The work also demonstrates the device capability to conduct temperature-dependent measurements down to pL droplet volumes by conducting a volume analysis given the dimensions of heaters used, independent of droplet boundary conditions. Sensitivity and uncertainty analyses based on these heater dimensions and surrounding material stack show the detection capabilities of these heaters, as they are optimally designed to maximize signal while accommodating the size restrictions of small volume droplets.

INTRODUCTION

Efforts in the biological community to optimize methodologies such as PCR and characterize biological reactions and processes have motivated continued reductions in sample volume. As volumes decrease, traditional detection techniques are becoming increasingly difficult, and thermal alternatives offer the potential to further reduce required sample volumes and provide a means to detect very small thermal perturbations to the system. DNA, for example, is conventionally detected using fluorescence for sequencing and

melt curve characterization. However, fluorescence detection is often costly and can be difficult when working with the small volumes and concentrations current PCR technology is striving towards. Thus, alternative based on thermometry are being explored for possible means of detection in order to both reduce cost and accommodate steadily decreasing sample volumes. Before exploring the application to DNA and other biological samples, however, thermometry techniques must be validated for known fluids with the target volume of interest.

Significant efforts have been made in the thermal community to characterize the thermal conductivity and heat capacity of fluids. Most fluid thermal characterization has been conducted on large volume samples, where traditional techniques such as the transient hot-wire technique [1, 2], calorimetry [3, 4], and 3ω [5, 6, 7, 8] have all been employed. These measurements can be extended to the small volume regime in order to aid in downscaled biological applications, which are constrained by feasible sample sizes and concentrations. In several works reporting values of fluid thermal properties using the 3ω method, many of the structures, such as those that utilize suspended wires [7, 8] are forced to be larger in dimensions (several millimeters in heater length) for the sake of stability and structural integrity of the heater wire. This limits the minimum sample volume size due to the heater wire's total immersion into a large fluid bath. Additionally, on-substrate devices [5, 6] that have performed 3ω to characterize room-temperature fluid thermal properties have ranged from 1-6mm in length, subsequently restricting the sample to larger volumes. Though groups have reported achievable minimum volumes of µL droplets [5], few have actually experimentally determined properties of such small volumes [9, 10]. Performing thermal measurements on microliter level and sub-microliter volumes offers a special challenge for metrology development, specifically when optimizing device design to both maximize sensitivity and meet the size restrictions that micro-, nano-, and pico-liter droplets introduce. While the 3ω method has been successfully demonstrated on micro- and nano-liter droplet volumes [9, 10], there is opportunity for further sensitivity optimization, allowing for very small signal detection, and extending the technique for even smaller sample volumes.

Though other works have characterized room-temperature thermal conductivity and heat capacity of micro-liter volume scale fluids, few report on the temperature-dependence of these properties. As many biological and phase change material reactions are temperature-induced, data for the temperature-dependent variation in the thermal properties of these fluids for such applications are critical. 3ω offers the opportunity to characterize the temperature-dependent thermal properties of µL volumes, which can ultimately be extended to such applications.

Here we apply the 3ω measurement technique to µL volumes and explore the limits that may apply when scaling down to pL sample sizes. We specifically investigate fluid samples of DI water, 10mM Tris/5mM HEPES buffer solution, and 1cSt silicone oil to experimentally determine their temperature-dependent thermal properties from room temperature (25°C) to 80°C. Comparison of these values of thermal conductivity κ and volumetric heat capacity C_v to available literature values demonstrate the accuracy of this technique when applied to µL samples. The work also indicates the devices' ability to conduct temperature-dependent measurements down to pL droplet volumes, as seen in Figure 1. Fig. 1 shows the results of a 2-dimensional numerical analysis to demonstrate the probed volumes for the heaters designed in this work, as compared to those used in literature. Further explanation of this plot can be found in the Results and Discussion section. Additionally, a sensitivity and error analysis based on these heater dimensions and surrounding material stack shows the detection capabilities of these heaters, as they are specifically designed to maximize signal while accommodating the size restrictions of µL droplets. These sensitivity capabilities, along with the ability to measure micro-to-picoliter volumes, demonstrate the potential of this methodology and geometry, specifically for biological processes and other applications, where detection of very small thermal perturbations in the system is necessary.

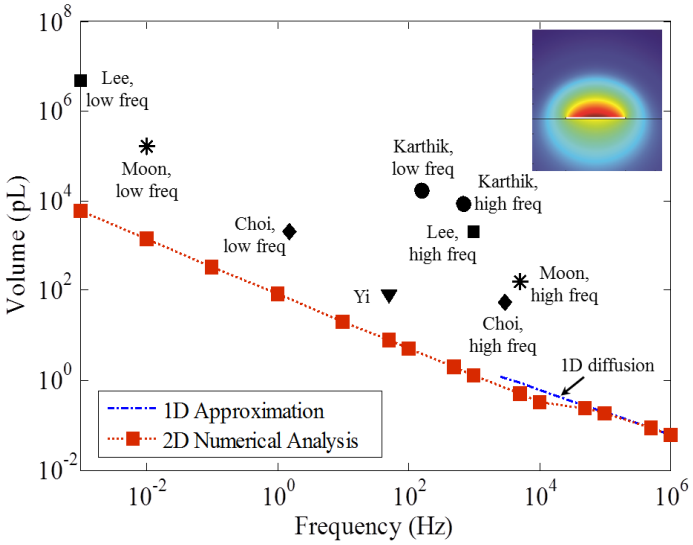

Fig. 1: Comparison of the liquid volumes examined by previously published papers, as determined using their reported heater geometries and measurement frequencies, as well as a 2D numerical analysis for the smallest heater (200µm length, 2µm width) used in this work.

EXPERIMENT

The measurement devices consist of metal heaters patterned onto a fused silica substrate, where the metal was deposited using e-beam evaporation (Innotec), with a 5nm titanium adhesion layer, followed by 60nm of platinum. The heater widths and lengths are designed to achieve the maximum measurement sensitivity possible within the constraints of photolithography techniques (2µm minimum resolution) and the small droplet and µL volumes. A 2µL droplet on a substrate has

an approximate diameter of 2mm; thus, to ensure the entire heater is contained under the fluid volume, heater lengths are restricted to less than 1mm for ease of droplet placement. The metal is patterned using standard photolithography techniques and lift-off, with heater widths ranging from 2µm to 5µm, and lengths ranging from 200µm to 700µm. The shorter heater lengths facilitate smaller droplets, while the higher aspect ratio heaters maximize the sensitivity resolution of the measurement. Figure 2 shows the layout of each device, containing two parallel heater lines of specific dimension, decoupled by a 100µm gap. Following the metal patterning, a 45nm oxide passivation layer is deposited using an Atomic Layer Deposition (ALD) process in order to prevent current leakage through the fluid, which is particularly significant for fluid and conductive material measurements. The ALD technique is used due to its conformal deposition, ensuring a high-quality thin film to electrically isolate the metal heaters from electrically conductive fluids, while not compromising thermal sensitivity. To provide probe tip access to the metal contact pads, a second lithography step is utilized to etch the oxide from the contact pads using a wet etch bath, as indicated in Figure 2B.

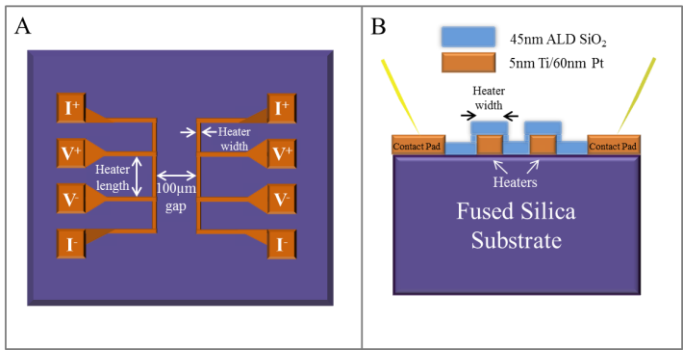

Fig. 2: (A) Top view of two decoupled parallel heater lines. (B) Cross-sectional view of device with 45nm ALD SiO_2 passivation layer etched away from metal contact pads to provide probe tip access.

The 3ω measurement consists of driving an AC current through a metal heater at frequency ω, which results in Joule heating and subsequent temperature oscillation in the heater line at frequency 2ω. The 3ω voltage captures the temperature rise seen by the heater, governed by the thermal properties of the surrounding materials stack, and can be used to extract thermal conductivity κ and volumetric heat capacity C_v of fluids. A more in-depth explanation of the 3ω method can be found in prior literature [11, 12]. Using the solution for thermal diffusion through a stratified media with a modulated heating source at an arbitrary point, the average temperature rise ΔT seen at the heater can be derived as:

$$\Delta T_{avg} = \frac{P}{2\pi L b^2}\int_0^{\infty} \frac{B^+(m)+B^-(m)}{A^+(m)B^-(m)-A^-(m)B^+(m)}\frac{sin^2(mb)}{\gamma_n m^2}dm \quad (1)$$

$$\gamma_n = \kappa_j\sqrt{m^2 - i\frac{\omega}{D_j}} \quad (2)$$

where P, L, and b are the heating power, length and width of the heater line, respectively. κ and D_j correspond to the out-of-plane thermal conductivity and diffusivity of layer j, η_j accounts for anisotropy, and $B^+(m)$, $B^-(m)$, $A^+(m)$, and $A^-(m)$ are dimensionless parameters solved by this recursive matrix method [13]. The experimental 3ω data is plotted in comparison to this analytical solution, and parameters are determined using a least squares fit algorithm. The 3ω measurement is carried out in the frequency domain, sweeping through frequencies of 400Hz to 2.4kHz, where the minimum diffusion depth is well beyond the thickness of the 45nm oxide film, but the sample volume and fused silica substrate are semi-infinite from the perspective of the heater with an approximate maximum thermal penetration of 19µm. This frequency range is chosen in particular to investigate smaller fluid volumes, dictated by the frequency-dependent radial thermal penetration. An initial measurement on passivation over metal is done to calibrate and verify the measurement rig, as well as characterize parameters including heater width, oxide passivation thickness and thermal properties, and fused silica substrate thermal properties. Though the nominal oxide thickness is determined using an ellipsometer after fabrication, the oxide film thickness and heater width variation (due to lift-off effects) is calibrated for each heater. It is essential to characterize any deviance from the nominal heater width, as this will affect the resistance of the heater and the subsequent temperature rise and 3ω signal.

Droplets of volume 2µL are used for the DI water and buffer solution, while a bulk volume of 15µL is used for silicone oil. These respective volumes are chosen based on the likelihood of evaporation during the temperature-dependent measurement. To prevent evaporation of the DI water and buffer solutions, 20µL of mineral oil is placed on top of the droplets; however, as the silicone oil sample used is very low viscosity (1cSt), it does not share the same segregate properties with water or other oils, so a larger bulk volume must be measured to preserve the sample during the duration of measurement. To contain the fluid, an acrylic well of dimensions 3.5mm x 3.5mm x 5mm(height) is fixed to the substrate using a thin layer of epoxy. The µL volumes of fluid sample are placed on the oxide surface via pipetting, such that the droplet and volume areas cover the entire heater length, which is imperative for temperature uniformity. A heater of dimensions 700µm length and 4µm width is used for all three fluids.

RESULTS AND DISCUSSION

In order to attain accurate values for the temperature-dependent properties of the fluid samples, a preliminary measurement is made to characterize the temperature-dependent thermal conductivity and volumetric heat capacity of the fused silica substrate, shown by Figure 3. The analytical solution is

seen to be thermally insensitive to the ALD SiO_2 passivation; thus, literature values were taken for the SiO_2 film properties. The curve fitting technique used to achieve unique sensitivity to both κ and C_v is discussed below in the uncertainty analysis, which contributes to the main source of uncertainty in individual property characterization. While it is often difficult to extract both κ and C_v using traditional 3ω with large width heaters, the reduced lateral dimensions of the heaters used in this work provide independent sensitivity to κ and C_v. However, in this case, the multiple parameter fit comes at the expense of increased uncertainty in the measured values as compared to data extraction when there are fewer independent unknown variables.

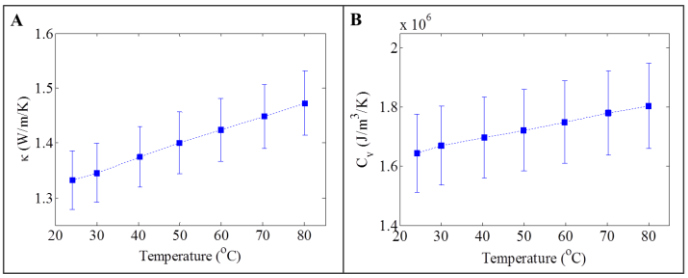

Fig. 3: Temperature-dependent thermal conductivity (A) and volumetric heat capacity (B) of the fused silica substrate. Uncertainty bars due to least squares fitting algorithm, discussed below in the Uncertainty Analysis.

Following the temperature-dependent characterization of the substrate materials, 3ω was performed on each of the three fluid samples from 24°C to 80°C. The thermal properties found for the substrate materials at each temperature were used when fitting for the thermal properties of the fluids to isolate the contribution of fluid changes due to temperature alone. The room temperature characteristics of DI water and silicone oil are compiled in Table I and compared to literature values. Good agreement was seen for each sample, with errors below 1% for both κ and C_v. Literature values for the 10mM Tris/5mM HEPES solution is not readily available.

	κ (W/m/K) Experimental	C_v (J/m^3/K) Experimental	κ (W/m/K) Literature	C_v (J/m^3/K) Literature	% Error $(d\kappa/\kappa)/(dC_v/C_v)$
DI Water	0.6043	4.1686e6	0.6051[CINDAS]	4.1716e6	0.13/0.07
Silicone Oil	.0991	1.6462e6	0.1[OMTS]	1.64e6[OMTS]	0.8/0.25

Table I: Room temperature thermal properties of DI Water and Silicone Oil compared to literature values.

Figure 4 illustrates the temperature dependent trends, showing κ and C_v data for DI water, the buffer solution, and the silicone oil, with the comparison of temperature-dependent literature values of DI water κ. Since there is no temperature-dependent literature readily available for the silicone oil (above room temperature), the oil trends were compared to fluorinated oil, for which there is temperature-dependent literature on thermal properties. Due to their similarities in viscosities and molecular weight, their temperature-dependent trends in thermal conductivity, density, and specific heat should follow closely. The fluorinated oil was seen to decrease in thermal conductivity with increasing temperature, which is confirmed by the trend seen in the silicone oil in Figure 4(E). The specific heat and density of fluorinated oil have opposing trends; however, the overall effect in volumetric heat capacity is dominated by the decreasing density as temperature rises, leading to the trend in silicone oil seen in Figure 4(F).

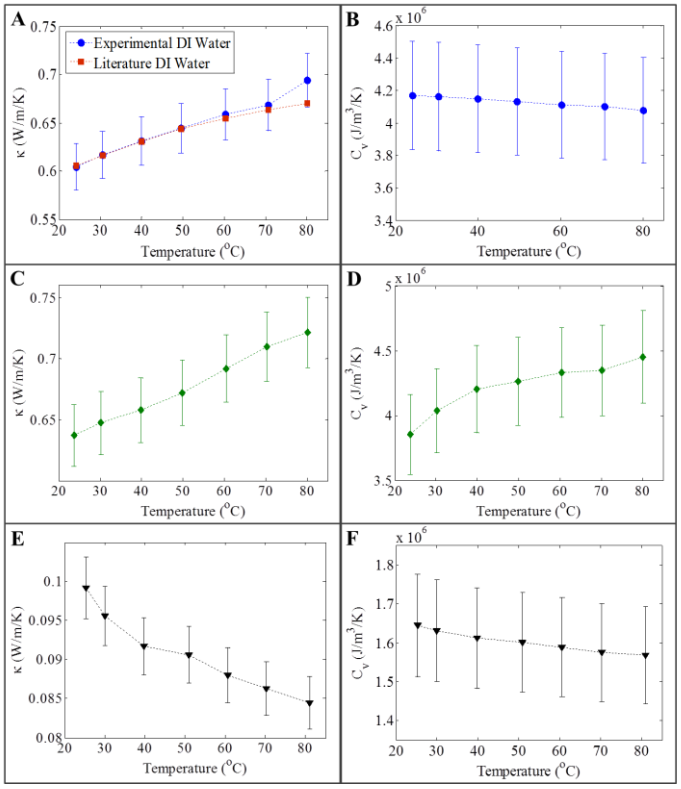

Fig. 4: Temperature-dependent thermal conductivity and volumetric heat capacity of DI water, (A) and (B), 10mM Tris/5mM HEPES buffer, (C) and (D), and 1cSt silicone oil, (E) and (F), respectively.

Volume Analysis

Though volumes of 2μL, 2μL, and 15μL were used for the DI water, buffer solution, and silicone oil, respectively, the actual volume being probed is significantly smaller, depending on heater geometries and frequency-dependent thermal penetration into the fluid. In the low-frequency limit, due to the quasi-steady-state conditions of the 3ω measurement, heat diffusion is limited by lateral spreading from the heater and dictated significantly by the heater width dimension. Conversely, at the high-frequency limit, heat diffusion reduces to 1-dimensional thermal propagation, so the thermal penetration depth is dictated by $l = \sqrt{\propto/(2\pi f)}$, where heating occurs on the 2nd harmonic of f, and α is the thermal diffusivity of the fluid. The high-frequency regime with 1-D thermal

penetration begins to dominate when the amplitude of heating approximately reduces to $(1/e)\cdot\Delta T$ at a depth equal to or less than half the heater width, where ΔT is the temperature change at the surface of the heater. Figure 5 illustrates these differing operating regimes and indicates the volumes probed as a function of frequency for this work, using the smallest designed heater of width 2µm and length 200µm, as well as other works in the literature which use traditional 3ω to analyze fluid thermal properties. At the low-frequency limit, the measured volume is approximately dictated by the half-volume of a cylinder, $V_{LF} = 0.5\cdot\pi\cdot l_{heater}\cdot r_{2Dpen}^2$, where l_{heater} is the heater length, and r_{2Dpen} is the numerically calculated radial penetration depth. When r_{2Dpen} is smaller than the half-width of the heater, the probed volume is dictated by the product of the length, width, and 1-dimensional thermal penetration of the heater ($V_{HF} = 200\mu m\cdot 2\mu m\cdot r_{1Dpen}$), as it is necessary for the entire length of the heater to be contained under the droplet volume for temperature uniformity. The effective volume probed in this work and quoted in Fig. 5 is determined using the low-frequency volume expression until 1-dimensional thermal diffusion begins to dominate at higher frequencies, at which point the thermal penetration depth reaches a depth that is less than the heater half-width. Figure 5 shows representative temperature fields illustrating the behavior of the thermal penetration depth while accounting for radial spreading for each regime, calculated from finite element solution (COMSOL) and using the smallest heater geometry of 200µm in length and 2µm in width, with the thermal properties of water above the heater, and those of silicon dioxide below to simulate the fused silica substrate. To quantify the thermal penetration depth, accounting for radial spreading effects, a numerical calculation was performed using the expression in Eq. (3), derived from the radial solution seen in Carslaw and Jaeger [11, 14] for an infinitely thin heater. The thermal penetration at x=0 (at the center of heater) is found by integrating along the width of the heater:

$$\Delta T = \int_{-b}^{b} \frac{P}{l\pi\kappa}\cdot \mathrm{K}_0\left(q\sqrt{x^2+y^2}\right)dx, \qquad (3)$$

where b is the half-width of the heater, P/l is the power per unit length generated by the line heater, κ is the thermal conductivity of the semi-infinite layer (DI water, in this case), and K_0 is the 0^{th} order Bessel function of the quantity qr, or $q\sqrt{x^2+y^2}$, where q is the complex thermal wave number defined by:

$$q = \sqrt{\frac{i2\omega\rho c_p}{\kappa}} \qquad (4)$$

where ρ, c_p and κ are the density, specific heat, and thermal conductivity of the semi-infinite layer, respectively [6]. For a given heater half-width and operating frequency, the 2-D thermal penetration can be defined as the y-depth at x=0 where the amplitude of the oscillating temperature is $(1/e)\cdot\Delta T$, where ΔT is the temperature rise at the surface of the heater.

Other groups who have performed small volume measurements using 3ω cite larger volumes as their minimum sample size; however, the same 2D and volume analysis was performed on these works as well, using their smallest feasible heater geometries and the extreme limits of their specified frequency ranges, and are included in Figure 5 for comparison. The comparison shows that due to large heater design, most other published works are forced to either probe larger volumes if lower frequencies are needed, or operate in the high frequency regime. The heaters in this work offer the unique opportunity to work in both the high and low frequency regimes while measuring a volume of less than 10nL. This flexibility in frequency of heating while consistently probing such small volumes is potentially very useful for many biological applications, where reaction kinetics can vary dramatically and sample sizes are traditionally small.

Sensitivity and Uncertainty Analysis

One of the challenges of extending measurement techniques down to small volume regimes is maintaining measurement accuracy and sensitivity comparable to those in the larger volume samples. Most 3ω measurements conducted on microliter and sub-microliter volume samples are restricted in part by the width and length of the heaters themselves while not compromising the sensitivity of the measurement. Measurement sensitivity is largely controlled by the aspect ratio of the heaters, where a larger length to width ratio allows for great signal-to-noise detection capability by decreasing the dT/dR of the heater. Since the temperature oscillations at the surface of the heater can be calculated from the expression, [11]:

$$\Delta T = 2\frac{V_{3\omega}}{I}\frac{dT}{dR} \qquad (5)$$

minimizing the value of dT/dR will maximize the 3ω voltage signal and reduce the detectable ΔT. A local sensitivity analysis is performed on a range of heater geometries designed for this measurement, with lengths of 700µm and widths ranging from 2µm to 5µm, varying either the thermal conductivity or volumetric heat capacity of the semi-infinite fluid above the heater to understand the independent contribution of both parameters to a variation in ΔT, as seen in the terms defined in Equation 6:

$$\left|\frac{\partial T}{\partial \kappa}\right| \Rightarrow \frac{\Delta\kappa}{\kappa}, \quad \left|\frac{\partial T}{\partial C_v}\right| \Rightarrow \frac{\Delta C_v}{C_v} \qquad (6)$$

The minimum changes in κ and C_v are characterized by following the analysis shown in Eq. 6 and determining the percent change in each that independently contributed to the minimum uncertainty in ∂T. The uncertainty in ∂T is determined by both the uncertainty in dT/dR and the frequency-dependent signal-to-noise ratio (SNR) of the equipment. When characterizing individual parameters, the primary source of

error is due to the measured value of *dT/dR*, an intrinsic characteristic of the heater line. To correctly characterize the value and variation of *dT/dR* of the heater line, multiple temperature vs. resistance sweeps are taken with the measurement heater at both low and high driving currents [11]. At lower frequencies, where the SNR of the system is low, the uncertainty in *dT* is dominated by the uncertainty in *dT/dR* measurements, found to be about ±0.77% and corresponding to a minimal detectable temperature of ±28.8mK at 1Hz and ±11.9mK at 1kHz. At high-frequency limits, however, the contribution of *dT/dR* is minimal, and system-level noise begins to dominate due to the low signal levels, leading to a noise contribution of ±0.5mK at 100kHz.

A second analysis is also performed to demonstrate a hypothetical geometry for further optimizing sensitivity while maintaining the small volume regime of this measurement. The suggested geometry is a microchannel of height 50µm and width 150µm, where both the substrate and channel enclosure are PDMS, and heaters of the same dimensions as this work are used (700µm length, 2-5µm width). Using a substrate material such as PDMS or a comparable polymer, where κ is approximately 1/10th that of oxide, forces more heat conduction through the sample above due to the thermally-insulating substrate, thereby enabling measurement of even smaller changes in κ and C_v. Figure 6 illustrates the results of both of these geometries, that of this work and the hypothetical stack, for frequencies of 1Hz, 1kHz, and 100kHz; the filled markers indicate the geometry used in this work, with the fused silica substrate, while the open markers indicate the hypothetical geometry, with the PDMS substrate and microchannel. For each frequency regime and type of substrate, the minimum detectable changes in κ (thermal conductivity, Fig. 6(A)) and C_v (volumetric heat capacity, Fig. 6(B)) are calculated independently for 4 heaters, with lengths 700µm and widths ranging from 2µm to 5µm. The variation in widths is reflected in the volumes probed by the heater, where the widest heater corresponds to the largest volume within each frequency regime. Figure 6 demonstrates that even with the presence of the fused silica substrate, very small changes in both κ and C_v can be detected for a wide range of frequencies, all while probing sub-µL volumes. The hypothetical optimization of substrate material does improve the sensitivity dramatically, specifically in the low-frequency regime.

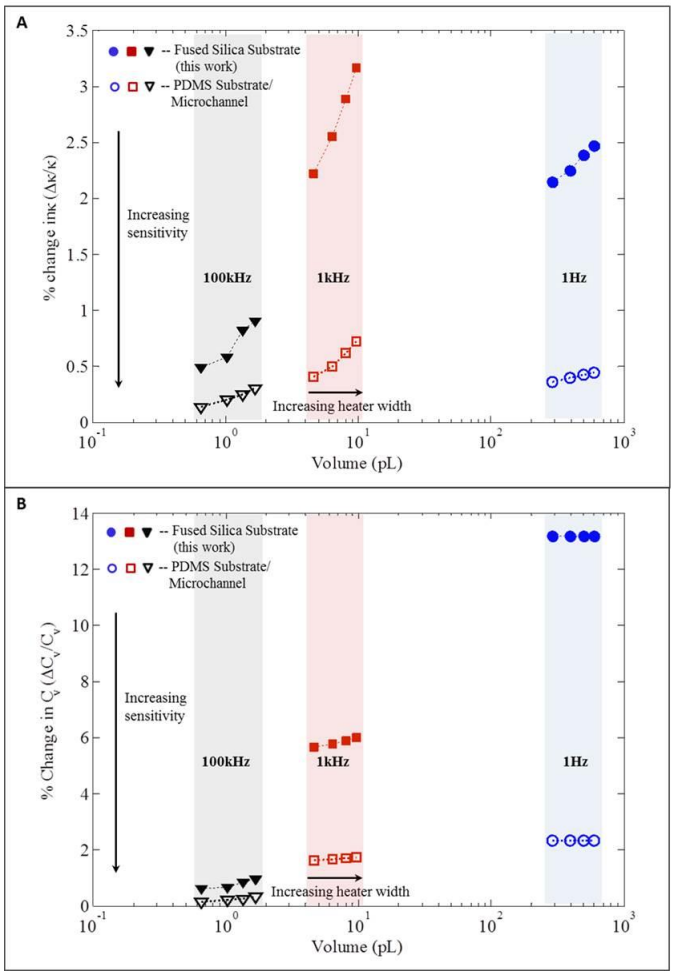

Fig. 5: Sensitivity analysis for thermal conductivity κ and volumetric heat capacity C_v for frequency regimes 1Hz, 1kHz, and 100kHz. Points are indicative of minimum detectable individual thermal properties based on frequency-dependent system error. All heater lengths are 700µm, and widths range from 2µm to 5µm. The filled markers indicate the geometry used in this work, with the fused silica substrate; open markers indicate the suggested optimized microchannel geometry with PDMS substrate. Width variation is reflected in the volumes probed by the heater; the widest heater corresponds to the largest volume within each frequency regime.

An uncertainty analysis is also performed to understand the abilities of the least squares algorithm to fit uniquely for both κ and C_v, which dominates the uncertainty bars in the temperature-dependent results. The uncertainty analysis fixes the value of one of the two parameters to be characterized (either κ or C_v), while allowing the least squares algorithm to fit freely for the other parameter. Following this optimization, the sum of the squares of the residuals is normalized to the sum of the squares of the temperature profile and reflected as a % Error (eq. 7):

$$\% \; Error = \frac{\Delta\epsilon}{\epsilon} = \sqrt{\frac{\sum_{i=1}^{n} r_i^{\,2}}{(\Delta T)^2}} \qquad (7)$$

Figure 6 reflects the uncertainty while fixing κ (A) and C_v (B); from the analysis, it is seen that within ±4% of the nominal value of κ, it is difficult to garner a truly unique fit without prior knowledge of the value of C_v. Beyond this threshold, analytical deviation rises rapidly. The same effect is observed within ±8% of the nominal value of C_v in Figure 6B. However, we see opposing trends within the flat regimes of both (A) and (B), indicating that we are in fact sensitive to the effusivity of the fluid. This effect, as well as additional optimization can also be utilized to independently characterize each parameter by measuring the sample with two different heater widths, thus narrowing the range of the optimal fit.

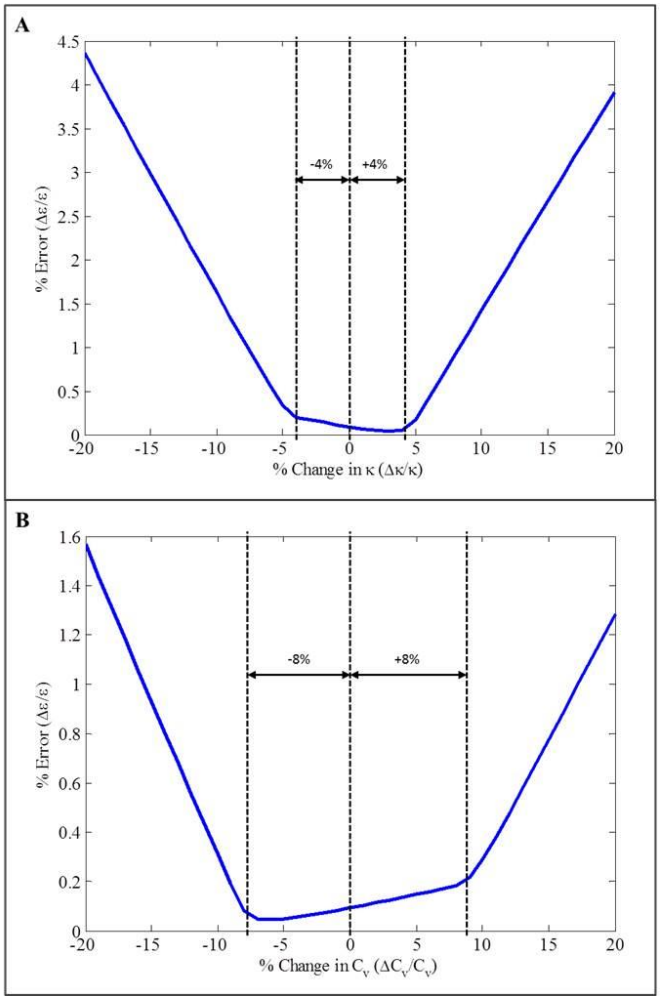

Fig. 6: Uncertainty analysis performed with least squares fitting algorithm for both κ and C_v, individually. Percent deviation of (A) κ, and (B) C_v, respectively, are held constant while optimizing for the second parameter; error is reported in the percentage deviation in the normalized sum of the squared temperature residuals.

CONCLUDING REMARKS

In this work, a 3ω methodology for measuring the temperature-dependent thermal properties, κ and C_v, of small volume fluids is proposed, specifically focusing on maximizing the heaters' sensitivity capabilities while probing nanoliter and sub-nanoliter volumes at both high and low frequency regimes. A sensitivity analysis shows the smallest perturbations in κ and C_v that can be detected by the range of heaters and fused silica substrate used in this work; depending on the heating frequency, changes in κ and C_v as small as 0.5% can feasibly be detected. The sensitivity analysis also suggests a hypothetical geometry with identical heater sizes, but with a substrate and microchannel fabricated from PDMS, thus increasing the detection capabilities significantly, specifically at the low frequency limit. A volume analysis and comparison is also performed with this work's heater geometries and those that exist in the literature, demonstrating the ability of these heaters to probe significantly smaller volumes than those in other works, which are forced to operate at higher frequencies in order to probe volumes of the same order. The sensitivity and small volume capabilities of this work's heaters offer an improved detection mechanism for biological reactions in particular, where flexibility in frequency is required while minimizing volume and maximizing sensitivity.

ACKNOWLEDGMENTS

Acknowledgments to Tim English from Stanford University Mechanical Engineering for ALD deposition support, and Bio-Rad Laboratories for supplying silicone oil samples. The authors gratefully acknowledge the financial support of the National Science Foundation Graduate Research Fellowship, as well as the Semiconductor Research Corporation (SRC) through task 2252.001.

REFERENCES

[1] Roder, H. M., 1981, "A transient hot wire thermal conductivity apparatus for fluids," J. Res. Natl. Bur. Stand 86: 457-493.

[2] Nagasaka, Y., and Nagashima, A., 1981, "Absolute measurement of the thermal conductivity of electrically conducting liquids by the transient hot-wire method," Journal of Physics E: Scientific Instruments 14.12: 1435.

[3] Garden, J-L., Château, E., and Chaussy, J., 2004, "Highly sensitive ac nanocalorimeter for microliter-scale liquids or biological samples," Applied physics letters 84.18: 3597-3599.

[4] Lee, W., et al., 2009, "High-sensitivity microfluidic calorimeters for biological and chemical applications,"

Proceedings of the National Academy of Sciences 106.36: 15225-15230.

[5] Choi, S. R., Kim, J., and Kim, D., 2007, "3ω method to measure thermal properties of electrically conducting small-volume liquid," Review of Scientific Instruments 78.8: 084902-084902.

[6] Moon, I. K., Jeong, Y. H., et al., 1996, "The 3ω technique for measuring dynamic specific heat and thermal conductivity of a liquid or solid," Review of Scientific Instruments **67**(1): 29-35.

[7] Karthik, R., N., Nagarajan, H., et al., 2012, "Measurement of thermal conductivity of fluids using 3-ω method in a suspended micro wire," Journal of Engineering Thermophysics **21**(1): 60-68.

[8] Lee, S.-M., 2009, "Thermal conductivity measurement of fluids using the 3ω method," Review of Scientific Instruments **80**(2): 024901-024901-024907.

[9] Choi, S. R., Kim, J., et al., 2007, "3ω method to measure thermal properties of electrically conducting small-volume liquid," Review of Scientific Instruments **78**(8): 084902-084902-084906.

[10] Yi, N., Park, B. K., et al., 2011, "Micro-droplet detection and characterization using thermal responses," Lab on a Chip **11**(14): 2378-2384.

[11] Cahill, D. G., 1990, "Thermal conductivity measurement from 30 to 750 K: the 3ω method," Review of Scientific Instruments **61**(2): 802-808.

[12] Dames, C., and Chen, G., 2005, "1ω, 2ω, 3ω," Review of Scientific Instruments 76.12: 124902-124902.

[13] Kim, J. H., Feldman, A. et al., 1999, "Application of the three omega thermal conductivity measurement method to a film on a substrate of finite thickness," Journal of Applied Physics **86**(7): 3959-3963.

[14] Carslaw, H. S., and Jaeger, J. C., 1959, "Conduction of Heat in Solids (paperback)."